Electronic structure and magnetic and optical properties of double perovskite Bi_2FeCrO_6 from first-principles investigation*

Song Zhe-Wen(宋哲文)[a)b)] and Liu Bang-Gui(刘邦贵)[a)†]

[a)] *Beijing National Laboratory for Condensed Matter Physics, Institute of Physics, Chinese Academy of Sciences, Beijing* 100190, *China*
[b)] *School of Physics, Peking University, Beijing* 100871, *China*

(Received 3 December 2012; revised manuscript received 6 January 2013)

Double perovskite Bi_2FeCrO_6, related with multiferroic $BiFeO_3$, is very interesting because of its strong ferroelectricity and high magnetic Curie temperature beyond room temperature. We investigate its electronic structure and magnetic and optical properties by using a full-potential density-functional method. Our optimization shows that it is a robust ferrimagnetic semiconductor. This nonmetallic phase is formed due to crystal field splitting and spin exchange splitting, in contrast to previous studies. Spin exchange constants and optical properties are calculated. Our Monte Carlo magnetic Curie temperature is 450 K, much higher than any previously calculated value and consistent with experimental results. Our study and analysis reveal that the main magnetic mechanism is an antiferromagnetic superexchange between Fe and Cr over the intermediate O atom. These results are useful in understanding such perovskite materials and exploring their potential applications.

Keywords: magnetic materials, first principles calculation

PACS: 75.50.–y, 71.20.–b, 75.10.–b, 85.75.–d **DOI:** 10.1088/1674-1056/22/4/047506

1. Introduction

It has been established that ferroelectricity and magnetism can coexist above room temperature in $BiFeO_3$ materials.[1–3] Actually, magnetic materials keeping high spin polarization at room temperature or higher are highly desirable for spintronic applications.[4,5] Half-metallic materials[6] and ferromagnetic (or ferrimagnetic) semiconductors are intensively studied for this purpose. Up to 96% spin polarization has been achieved experimentally in the cases of (La,Sr)MnO_3 and CrO_2 materials.[5,7] Since 1998, double perovskite oxides have been extensively explored. Macroscopic magnetization and electric polarization beyond room temperature have been found in such materials.[8–12] Furthermore, high quality samples of semiconductor technology standard have been achieved for some of these compounds.[13] These stimulate world-wide interest in exploring multiferroic materials, especially those with macroscopic magnetization and electric polarization beyond room temperature, for novel devices.[1–3,14]

Double perovskite Bi_2FeCrO_6 can be constructed from $BiFeO_3$. It was predicted to have both ferroelectricity and ferrimagnetism, with theoretical electric polarization 80 $\mu C/cm^2$ and magnetic Curie temperature below 130 K.[15,16] Subsequently, the Bi_2FeCrO_6 was synthesized successfully by several groups, and experimental measurements on good samples revealed electric polarization up to 60 $\mu C/cm^2$ and magnetic Curie temperature well above room temperature.[17–23] The best experimental Curie temperatures are much higher than the first-principles predicted one, while the electric polarization is consistent between theory and experiment. Reasonable explanation of this contradiction is highly desirable to understand the basic physics of such materials and in exploring their applications.

In this paper, we combine a full-potential density functional theory (DFT) method with Monte Carlo simulation to investigate double perovskite Bi_2FeCrO_6, with emphasis on its electronic structure and magnetic Curie temperature. We first optimize its structure with generalized gradient approximation (GGA) and then study its electronic structure. We show that the resultant ferrimagnetic semiconductor phase is robust against both change of exchange–correlation potential and variation of structural parameters. Furthermore, we calculate spin exchange constants and thereby determine the magnetic Curie temperature. Our *ab initio* magnetic Curie temperature is 450 K, much higher than the previous DFT-based value but consistent with experimental results. In addition, we present calculated optical properties. The magnetic mechanism is understood in terms of the electronic properties. More detailed results will be presented in the following.

The rest of this paper is organized as follows. In the next section, we describe our computational details. In the third section we describe first-principles structural optimization and present our optimized results. In the fourth section we present the main first-principles electronic structures. In the fifth section we present first-principles magnetic calculations and re-

*Project supported by the National Natural Science Foundation of China (Grant Nos. 11174359 and 10874232) and by the National Basic Research Program of China (Grant No. 2012CB932302).

†Corresponding author. E-mail: bgliu@iphy.ac.cn

© 2013 Chinese Physical Society and IOP Publishing Ltd

sulting Curie temperature. In the sixth section we present first-principles optical properties. In the seventh section we make some necessary discussions. Finally, we give our conclusion in the eighth section.

2. Computational details

We use the full-potential augmented plane wave method within the density functional theory (DFT),[24,25] as implemented in package WIEN2k.[26] Generalized gradient approximation[27] is used for the exchange–correlation potential for calculating our main results, and local density approximation (LDA)[28] and a modified Becke–Johnson exchange potential (mBJ)[29] are also used for comparative calculations. Full relativistic effects are calculated with the Dirac equations for core states, and the scalar relativistic approximation is used for the other states.[30–32] The spin–orbit coupling is neglected because it has little effect on our main conclusion (to be detailed in the following). The muffin-tin radii of Bi, Fe, Cr, and O are set to 2.13, 1.84, 1.84, and 1.64 bohr. The spherical expansion in the muffin-tin spheres is done up to $l_{\max} = 10$. The parameter $R_{\rm mt} \times K_{\max}$ is set to 7.5. We use 1500 k-points in the first Brillouin zone (226 k-points in the irreducible Brillouin zone) during the calculations. The self-consistent calculations are considered to be converged only when the integration of absolute charge-density difference per formula unit between the successive loops is less than $0.0001|e|$, where e is the electron charge.

Metropolis algorithm and variants are used for our Monte Carlo simulations of classical approximation to the effective spin Hamiltonian.[33,34] Several three-dimensional lattices of up to $30 \times 30 \times 30$ NaCl unit cells with periodic boundary condition are used in these calculations. The first 5×10^4 Monte Carlo steps (MCS) of total 10^5 MCS are used for the thermal equilibrium, and the remaining 5×10^4 MCS are used for a given temperature. The $T_{\rm c}$ value is determined through investigating the average magnetization and magnetic susceptibility as functions of temperature.[33]

3. Structural optimization

It has already been proved[15,16] that the lowest energy structure of double perovskite Bi_2FeCrO_6 has $R3$ symmetry (space group # 146). Its structural difference from the cubic double perovskite is mainly due to the alternating rotations of oxygen octahedra around Fe/Cr cations. The magnetic order turns out to be ferrimagnetic with every Cr spin orienting upward and every Fe spin downward. We use experimental lattice constant $a = 5.537$ Å (1 Å = 0.1 nm) and $c = 13.502$ Å ($\alpha = 60.20°$) which are intermediate values of existing experimental results.[17–23] After internal structure optimization, every atom has a displacement from that of the cubic perovskite structure. We show its crystal structure in Fig. 1. The optimized parameters are summarized in Table 1. The bond lengths and Fe–O–Cr bond angle can be calculated from the structural parameters. The calculated values are summarized in Table 2.

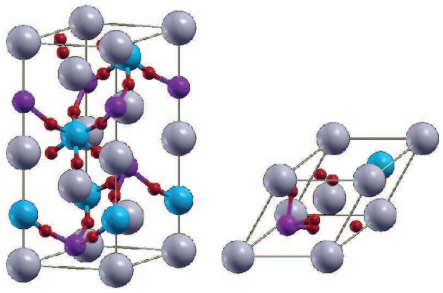


Fig. 1. (color online) The $R3$ (#146) crystal structure of double perovskite Bi_2FeCrO_6. The right-side is the primitive cell, and the left-side is used to describe the relative positions of the atoms. O is denoted by the smallest ball with red or black, Fe by the next-smallest ball with purple or black, Cr by the next-biggest ball with cyan or dark grey, and Bi by the biggest ball with grey.

Table 1. Optimized internal structural parameters of double perovskite Bi_2FeCrO_6 with the $R3$ (#146) crystal structure.

Atom	Parameter	Values
Bi	z_1	0.0005, 0.5040
Fe/Cr	z_2	0.7330/0.2260
O	x	0.5433, 0.0511
	y	0.9542, 0.9043
	z	0.3937, 0.4459

Table 2. Bond lengths (in unit Å) and Fe–O–Cr angle (°) of double perovskite Bi_2FeCrO_6 with the $R3$ (#146) crystal structure.

Bond length	Fe–O	2.130, 1.971
	Cr–O	1.947, 1.994
	Bi–O	2.347, 2.387
		2.406, 2.416
Bond angle	Fe–O–Cr	153.7, 153.6

These structural parameters are not much different from the previous LDA-optimized results.[15,16] Actually, we obtain 55.2 μC/cm^2 for the sum $\sum_i z_i u_i$ of formal charge z_i times displacement u_i, using formal charges 3.0, 3.0, 3.0, and −2.0 for Bi, Fe, Cr, and O, respectively. This is almost the same as the corresponding value 55 μC/cm^2 in the literature.[15,16] Therefore, we believe that similar ferroelectric polarization can be calculated with the present structural parameters. The total magnetic moment is equivalent to 2 $\mu_{\rm B}$ per formula unit. Different magnetic moments, 3.70 $\mu_{\rm B}$ and −2.18 $\mu_{\rm B}$, are observed in the spheres of Fe and Cr atoms, and magnetic moments in the spheres of other atoms are tiny. Here, the negative sign for the Cr moment is because it is antiparallel to the Fe moment. These imply that Fe and Cr are both in the high spin states.

4. Electronic structure

With the optimized crystal structure, we can study the electronic structure of the Bi_2FeCrO_6. In Fig. 2 we present the spin-resolved total density of states (DOS) and partial DOS projected in the d states of Fe and Cr between –7.3 eV and 5 eV. The corresponding spin-dependent band structure is presented in Fig. 3. It is clear that the Bi_2FeCrO_6 is a ferrimagnetic semiconductor, in contrast with the ferrimagnetic metallic phase obtained in previous pseudo-potential LDA/GGA calculations.[15,16,35,36] LDA + U method, with $U = 3$ eV and $J = 0.8$ eV, was used to obtain a Mott–Hubbard insulating state, but such an insulating phase cannot yield high Curie temperature[15,16] and therefore is not right to describe this material. The previous ferrimagnetic metallic phase was caused mainly by the pseudo-potential method which does not take the core electrons into account. Our ferrimagnetic semiconductor phase should be more reliable because the core electrons are considered in our full-potential calculations.

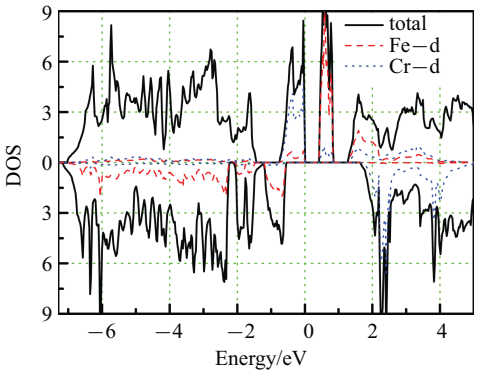


Fig. 2. (color online) Spin-resolved density of states (DOS, in state/eV per formula unit) of double perovskite Bi_2FeCrO_6, calculated with GGA. The solid line is total DOS, and dashed and dotted lines refer to partial DOS projected in the atomic spheres of Fe and Cr, respectively. The upper part in each panel is majority-spin DOS result, and the lower the minority-spin one.

In the majority-spin channel, the bands between –7.3 eV and –1.4 eV are from the 18 O 2p states; the three bands between –0.8 eV and 0 eV originate mainly from Cr 3d t2g; the three empty bands are almost Fe 3d t2g states; and the upper states are from Fe 3d eg, Cr 3d eg, and Bi 6p. In the minority-spin channel, the 23 filled bands are from 18 O 2p states and 5 Fe 3d ones; and the empty bands from Cr 3d and Bi 6p states. Here, the Fe 3d states hybridize with the O 2p and the Cr 3d ones interact strongly with the Bi 6p, in contrast to the majority-spin channel.

Because it is well known that both LDA and GGA underestimate the semiconductor gap, we use a new exchange potential, mBJ, to improve the electronic structure, especially the semiconductor gap. It has already been shown that this mBJ produces much better semiconductor gaps for not only usual semiconductors[29] but also magnetic semiconductors such as $LaMnO_3$ and $HgCr_2Se_4$ materials.[37–40] The mBJ DOS are presented in Fig. 4. The main features are similar to the GGA results, except that the mBJ gap is much wider than the LDA and GGA ones. The three semiconductor gaps are summarized in Table 3.

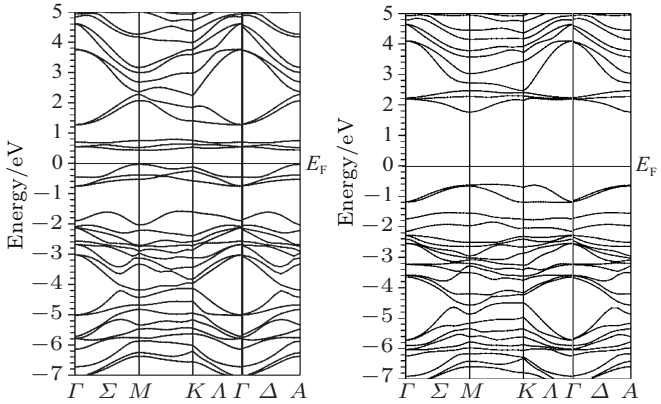


Fig. 3. Spin-resolved energy bands of double perovskite Bi_2FeCrO_6, calculated with GGA. The left-side panel is for majority-spin, and the right-side for minority-spin.

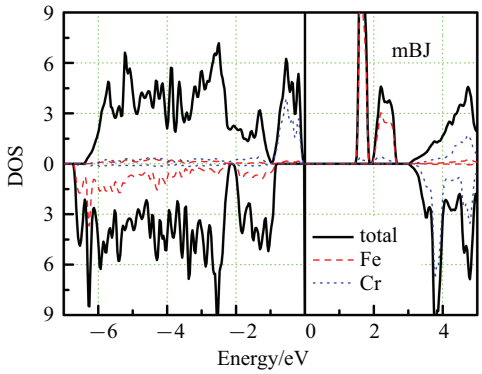


Fig. 4. (color online) Spin-resolved density of states (DOS, in state/eV per formula unit) of double perovskite Bi_2FeCrO_6, calculated with mBJ. The solid line is total DOS, and dashed and dotted lines refer to partial DOS projected in the atomic spheres of Fe and Cr, respectively. The upper part in each panel is majority-spin DOS result, and the lower the minority-spin one.

Table 3. The semiconductor energy gaps (in eV) of double perovskite Bi_2FeCrO_6, calculated with our optimized structure and previous one[15,16] in terms of LDA, GGA, and mBJ.

Structure	LDA	GGA	mBJ
This	0.26	0.42	1.48
Previous[15,16]	0.30	0.48	

Our study shows that this feature of ferrimagnetic semiconductor is robust to changes of crystal structure parameters. For example, the GGA and LDA gaps in the lower line of Table 3 are calculated with the previous structure parameters.[15,16]

5. Magnetic Curie temperature

In order to study spin exchange interactions, we compare the total energies of the four magnetic configurations in the

supercell consisting of 20 atoms, namely ferrimagnetic (the ground state) and ferromagnetic orders, and two other magnetic orders constructed by reversing one of the two Cr or Fe spins in the ferrimagnetic order. With respect to the ground state, the three magnetic structures have total energies: 310, 161, and 166 meV per formula unit, respectively. Because the induced spin density at the other atoms are very small compared to those at the magnetic atoms, we consider only Fe and Cr. The magnetic energies reflect the spin exchange energies e_{ij} where i and j denote two different spins. Fe and Cr atoms form a lattice of the NaCl crystal structure.[8,10,11,17,20] While the magnetic moments in the spheres of Fe and Cr are 3.70 μ_B and –2.18 μ_B, the Fe^{3+} and Cr^{3+} cations should contribute 5 μ_B and –3 μ_B, respectively. We can assign spin values $s = 5/2$ and $s = 3/2$ to the Fe and Cr spins, respectively. Therefore, we construct the effective spin Hamiltonian,

$$H = \sum_{\langle ij \rangle} J_{ij} \boldsymbol{S}_i \cdot \boldsymbol{S}_j, \tag{1}$$

where $\boldsymbol{S}_i$ is spin operator at site i (in both of the Fe and Cr sublattices), the summation is over spin pairs, and the spin exchange constant J_{ij} is limited to the nearest (Fe–Cr) and the next nearest (Fe–Fe and Cr–Cr) spin pairs. There exists a relation between the energies e_{ij} and constants J_{ij}, $e_{ij} = J_{ij} s_i s_j$, where s_i takes either $5/2$ or $3/2$. The total energy can be split into $E_0 + \sum_{\langle ij \rangle} e_{ij}$, where E_0 is defined to be independent of spin configuration. We obtain the following equations from the four magnetic structures

$$\begin{cases} 0 = E_0 - 6e_{\mathrm{Fe-Cr}} + 6e_{\mathrm{Fe-Fe}} + 6e_{\mathrm{Cr-Cr}}, \\ 310 = E_0 + 6e_{\mathrm{Fe-Cr}} + 6e_{\mathrm{Fe-Fe}} + 6e_{\mathrm{Cr-Cr}}, \\ 161 = E_0 + 6e_{\mathrm{Fe-Fe}}, \\ 166 = E_0 + 6e_{\mathrm{Cr-Cr}}. \end{cases} \tag{2}$$

We solve the e_{ij} parameters from the above equation set, and then calculate J_{ij} by using the above simple relation. The spin exchange energies e_{ij} and constants J_{ij} are summarized in Table 4.

Table 4. The calculated spin exchange energies (e_{ij}) and constants (J_{ij}) of double perovskite Bi_2FeCrO_6 for the nearest and next nearest spin pairs ($\langle ij \rangle$), and the resulting Curie temperature T_c from Monte Carlo simulation.

$\langle ij \rangle$	Fe–Cr	Fe–Fe	Cr–Cr
e_{ij}/meV	25.8	–1.88	–1.06
J_{ij}/meV	6.89	–0.30	–0.47
T_c/K	450		

We carry out Monte Carlo simulations of the Heisenberg model to estimate the T_c of the materials.[33,34] It is well known that Curie temperature will be a little underestimated if classical approximation to the Heisenberg model is used in the Monte Carlo simulation. We use Monte Carlo simulation of the classical Heisenberg model to give a lower bound for the Curie temperature of the quantum spin model. Our simulated average magnetization (in unit of 2 μ_B per Fe–Cr pair) as a function of temperature from classical Heisenberg model is presented in Fig. 5. Because the classical approximation is used, the low-temperature part is not very accurate with respect to the model, but the high-temperature part should be accurate enough to get reasonable Curie temperature. The calculated T_c value is equivalent to 450 K, meaning that real Curie temperature should be a little higher than 450 K. This Curie temperature is much higher than the original prediction (lower than 130 K),[15,16] but it is consistent with experimental high Curie temperatures beyond room temperature.[17,20–23]

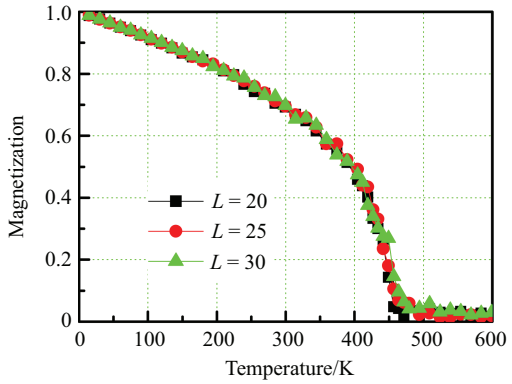


Fig. 5. (color online) Temperature-dependent magnetization (in units of 2 μ_B per Fe–Cr pair) of double perovskite Bi_2FeCrO_6, simulated with Monte Carlo method and the classical Heisenberg model.

6. Optical properties

Because optical properties are important to semiconductors, we calculate the direct electronic contributions of the optical dielectric function $\varepsilon(\omega)$ and optical conductivity $\sigma(\omega)$ curves of the Bi_2FeCrO_6 as functions of photon energy (ω). Considering that the semiconductor gaps have an important impact on the low-energy parts of these optical functions, we calculate them with both GGA and mBJ. These results, both real (Re) and imaginary parts (Im) between 0 eV and 12 (or 13) eV, are presented in Figs. 6 and 7.

For Re(ε), the GGA result of the low energy limit is substantially larger than the mBJ one, and both have a similar trend when the photon energy is larger than 1.5 eV. For Im(ε), the main difference appears for low energy (0 eV–1.5 eV). There is a sharp peak at 0.75 eV for the GGA result, which is related to the steep decrease in the GGA curve of Re(ε) at the same photon energy. The mBJ result of Im(ε) is equivalent to zero in this region, reflecting the broad semiconductor gap from mBJ. For higher energy, the results are similar. For the $\sigma(\omega)$ curves, the main difference also appears in the low energy region, Re($\sigma(\omega)$) having a peak approximately at 1.0 eV and Im($\sigma(\omega)$) having a valley approximately at 0.5 eV. For the

higher energy, the $\sigma(\omega)$ curves have similar behaviors. These calculated optical functions could be useful in exploring the optical properties of the Bi_2FeCrO_6 materials and others similar.

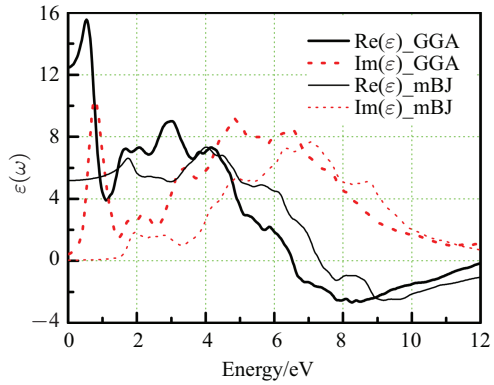


Fig. 6. (color online) Optical dielectric functions, both real (solid) and imaginary (dotted) parts, of double perovskite Bi_2FeCrO_6, calculated with GGA (thick) and mBJ (thin).

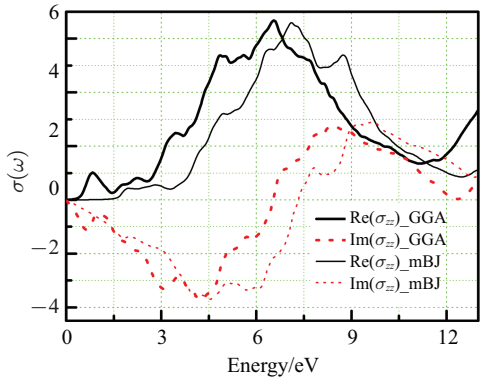


Fig. 7. (color online) Optical conductivity, both real (solid) and imaginary (dotted) parts, of double perovskite Bi_2FeCrO_6, calculated with GGA (thick) and mBJ (thin).

7. Discussions

Our DFT investigation with GGA, LDA, and mBJ shows that the ground-state phase of double perovskite Bi_2FeCrO_6 is a ferrimagnetic semiconductor with a clear semiconductor gap (larger than 0.26 eV), in contrast to previous ferrimagnetic metallic phases from LDA pseudo-potential calculations.[15,16,35,36] Even using the previous structural paramters,[15,16] we still obtain the ferrimagnetic semiconductor phase with both GGA and LDA. Furthermore, our spin exchange energies and interaction constants produce the high Curie temperature 450 K which is consistent with experimental high Curie temperature beyond room temperature.[17,20–23] This is in contrast to the previous LDA + U calculations which yield Mott–Hubbard insulator phases and low Curie temperatures (below 130 K).[15,16] These imply that we need not use LDA + U or GGA + U to achieve the reasonable ferrimagnetic semiconductor phase for double perovskite Bi_2FeCrO_6.

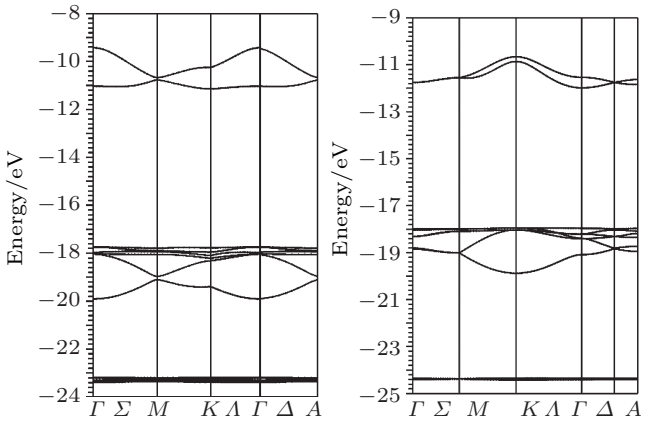


Fig. 8. The majority-spin part of the Bi 6s, O 2s, and Bi 5d energy bands of double perovskite Bi_2FeCrO_6 in the $R3$ (the left part) and cubic (the right part) structures, calculated with GGA.

Here, our semiconductor gap is formed between the filled Cr 3d t2g and the empty Fe 3d t2g bands. Essentially, it originates mainly from the crystal field splitting due to the deformation of the O octahedrons plus the spin exchange splitting of the 3d electrons. Our calculated spin exchange interaction between the nearest Fe and Cr atoms is positive, and the next nearest (Fe–Fe and Cr–Cr) ones are negative. These spin interactions become substantially weaker from the nearest to next nearest neighboring spin pairs, which implies that such a spin description is reliable. The main spin interaction is intermediated by the O atom in between the nearest Fe and Cr atoms. The Fe and Cr spins contribute opposite magnetic moments so that the ferrimagnetism is formed. Therefore, the main magnetic mechanism is the antiferromagnetic superexchange over the O atom.

Now we address possible contributions from deeper energy levels. For this purpose, we present in Fig. 8 the bands of Bi 6s, O 2s, and Bi 3d states of the R3 (space group #146) and cubic (space group #225) structures. They are below –9 eV from the Fermi levels. The Bi 5d bands (–23.3 eV or –24.4 eV) in both of the structures are completely flat, meaning that Bi 5d states are isolated, but there is a clear correlation between the two Bi 6s bands (from –11.0 eV to –9.4 eV) and two of the six O 2s ones (from –19.9 eV to –17.7 eV) in the case of the $R3$ structure. Noticeably, its Bi 6s bands are more separated from the O 2s ones than those of the cubic structure. This can be attributed to the expelling due to the small but nonzero hybridization of the two sets of s states. The interaction between the Bi 6s and O 2s states should be involved in the ferroelectric property in the $R3$ structure, because they are absent in the cubic structure without ferroelectricity.

8. Conclusion

In summary, we have investigated the electronic structure and magnetic and optical properties of double perovskite Bi_2FeCrO_6 by combining the full-potential augmented plane

wave method with Monte Carlo simulation. Our calculations show that our full-potential GGA-optimized phase is a ferrimagnetic semiconductor and it is robust against both change of exchange–correlation potential and variation of structural parameters. This nonmetallic phase is formed due to crystal field splitting and spin exchange splitting, in contrast to Mott–Hubbard insulating state in previous DFT studies. Spin exchange constants and optical properties are calculated. Our *ab initio* magnetic Curie temperature is 450 K, much higher than the previous DFT-based value but consistent with experimental results. Our study and analysis reveals that the main magnetic mechanism is an antiferromagnetic super-exchange between Fe and Cr over the intermediate O atom. Our results are useful in understanding such materials and exploring their potential applications.

References

[1] Wang J, Neaton J B, Zheng H, Nagarajan V, Ogale S B, Liu B, Viehland D, Vaithyanathan V, Schlom D G, Waghmare U V, Spaldin N A, Rabe K M, Wuttig M and Ramesh R 2003 *Science* **299** 1719
[2] Choi T, Lee S, Choi Y J, Kiryukhin V and Cheong S W 2009 *Science* **324** 63
[3] Ramazanoglu M, Laver M, Ratcliff II W, Watson S M, Chen W C, Jackson A, Kothapalli K, Lee S, Cheong S W and Kiryukhin1 V 2011 *Phys. Rev. Lett.* **107** 207206
[4] Wolf S A, Awschalom D D, Buhrman R A, Daughton J M, von Molnar S, Roukes M L, Chtchelkanova A Y and Treger D M 2001 *Science* **294** 1488
[5] Muller G M, Walowski J, Djordjevic M, Miao G X, Gupta A, Ramos A V, Gehrke K, Moshnyaga V, Samwer K, Schmalhorst J, Thomas A, Hutten A, Reiss G, Moodera J S and Munzenberg M 2009 *Nat. Mater.* **8** 56
[6] de Groot R A, Mueller F M, van Engen P G and Buschow K H J 1983 *Phys. Rev. Lett.* **50** 2024
[7] Park J H, Vescovo E, Kim H J, Kwon C, Ramesh R and Venkatesan T 1998 *Nature* **392** 794
[8] Kobayashi K I, Kimura T, Sawada H, Terakura K and Tokura Y 1998 *Nature* **395** 677
[9] Ueda T K K and Tabata H 1998 *Science* **280** 1064
[10] Serrate D, de Teresa J M and Ibarra M R 2007 *J. Phys.: Conden. Matter* **19** 023201 and references therein
[11] Opel M 2012 *J. Phys. D* **45** 033001 and references therein
[12] Boschker H, Kautz J, Houwman E P, Siemons W, Blank D H A, Huijben M, Koster G, Vailionis A and Rijnders G 2012 *Phys. Rev. Lett.* **109** 157207
[13] Hauser A J, Soliz J R, Dixit M, Williams R E A, Susner M A, Peters B, Mier L M, Gustafson T L, Sumption M D, Fraser H L, Woodward P M and Yang F Y 2012 *Phys. Rev. B* **85** 161201(R)
[14] Walker H C, Fabrizi F, Paolasini L, de Bergevin F, Herrero-Martin J, Boothroyd A T, Prabhakaran D and McMorrow D F 2011 *Science* **333** 1273
[15] Baettig P and Spaldin N A 2005 *Appl. Phys. Lett.* **86** 012505
[16] Baettig P, Ederer C and Spaldin N A 2005 *Phys. Rev. B* **72** 214105
[17] Nechache R, Harnagea C, Pignolet A, Normandin F, Veres T, Carignan L P and Menard D 2006 *Appl. Phys. Lett.* **89** 102902
[18] Suchomel M R, Thomas C I, Allix M, Rosseinsky M J, Fogg A M and Thomas M F 2007 *Appl. Phys. Lett.* **90** 112909
[19] Kim D H, Lee H N, Biegalski M D and Christen H M 2007 *Appl. Phys. Lett.* **91** 042906
[20] Kamba S, Nuzhnyy D, Nechache R, Zaveta K, Niznansk D, Santav E, Harnagea C and Pignolet A 2008 *Phys. Rev. B* **77** 104111
[21] Nechache R, Harnagea C, Carignan L P, Gautreau O, Pintilie L, Singh M P, Menard D, Fournier P, Alexe M and Pignolet A 2009 *J. Appl. Phys.* **105** 061621
[22] Aissa B, Nechache R, Therriault D, Rosei F and Nedil M 2011 *Appl. Phys. Lett.* **99** 183505
[23] Nechache R, Harnagea C and Pignolet A 2012 *J. Phys.: Condens. Matter* **24** 096001
[24] Hohenberg P and Kohn W 1964 *Phys. Rev.* **136** B864
[25] Kohn W and Sham L J 1965 *Phys. Rev.* **140** A1133
[26] Blaha P, Schwarz K, Sorantin P and Trickey S B 1990 *Comput. Phys. Commun.* **59** 399
[27] Perdew J P, Burke K and Ernzerhof M 1996 *Phys. Rev. Lett.* **77** 3865
[28] Perdew J P and Wang Y 1992 *Phys. Rev. B* **45** 13244
[29] Tran F and Blaha P 2009 *Phys. Rev. Lett.* **102** 226401
[30] MacDonald A H, Pickett W E and Koelling D D 1980 *J. Phys. C* **13** 2675
[31] Singh D 1994 *Plane Waves, Pseudopotentials and the LAPW Method* (Boston: Kluwer Academic)
[32] Kunes J, Novak P, Schmid R, Blaha P and Schwarz K 2001 *Phys. Rev. B* **64** 153102
[33] Metropolis N, Rosenbluth A W, Rosenbluth M N, Teller A M and Teller E 1953 *J. Chem. Phys.* **21** 1087
[34] Binder K and Heermann D W 2002 *Monte Carlo Simulation in Statistical Physics* (Berlin: Springer)
[35] Ju S and Guo G Y 2008 *Appl. Phys. Lett.* **92** 202504
[36] Goffinet M, Iniguez J and Ghosez P 2012 *Phys. Rev. B* **86** 024415
[37] Gong S and Liu B G 2011 *Phys. Lett. A* **375** 1477
[38] Gong S and Liu B G 2012 *Chin. Phys. B* **21** 057104
[39] Guo S D and Liu B G 2012 *Chin. Phys. B* **21** 017101
[40] Guo S D and Liu B G 2012 *J. Phys.: Condens. Matter* **24** 045502